Design, fabrication and actuation of four-axis thermal actuating image stabiliser

Chun-Ying Lin, Jin-Chen Chiou

Institute of Electrical and Control Engineering, National Chiao Tung University, Hsin-Chu, Taiwan
E-mail: sikun.ece95g@nctu.edu.tw

Published in Micro & Nano Letters; Received on 1st March 2011; Revised on 15th May 2011

Presented is a microelectromechanical system-based thermal actuating image stabiliser. The proposed stage has dimensions of $14.9 \times 14.9 \times 0.2$ mm^3 and contains a four-axis decoupling XY stage used for anti-shaking. The processes used to fabricate the stabiliser include silicon on isolator process, inductively coupled plasma process and flip-chip bonding technique. The maximum actuating distance of the stage is larger than 25 μm, which is sufficient to resolve the shaking problem in 3× optical zoom condition. According to the experiment results, the supplied voltage for the 25 μm moving distance is lower than 20 V, and the dynamic resonant frequency of the actuating device is 4.7 kHz.

1. Introduction: The manufacture of applications of the micro-electro-mechanical systems (MEMS)-based XY stage can now be realised by using micro/nano-fabrication processes due to advances in device miniaturisation and high precision systems [1]. In terms of the driving function of the MEMS-based XY stage, the comb-drive actuator plays a very important role in optical applications [2–9] and the probe positioning system [10], because it can be easily controlled and has highly precise position control and low power consumption. However, the driving voltage of electrostatic actuators is usually beyond 60 V, so the step-up circuit must be large enough to support the high voltage. To solve this problem, thermal actuating XY stages are researched, for example, the application of lens tracking and focusing [11].

Anti-shake technology is among the many new technologies developed for mobile phones, and image stabilisation is the typical solution to this problem. Among the familiar elements of image stabilisation are lens shifting, charge-coupled device shifting and signal processing. The conventional anti-shaking technique in digital single-lens reflexes, signal processing, is now used in mobile phones. Although signal processing requires no additional hardware and does not affect miniaturisation of the system module, performance and reliability depend on the algorithm used. Given the demand for device miniaturisation, the lens shifting anti-shaking approach is inadequate since adding a movable lens causes nonlinearity, which must be corrected by a complex control algorithm. Although it requires an associated actuating system, image sensor (IS) shifting is less disruptive of miniaturisation; the overall size of the system is also easier to reduce compared to the lens shifting method. For the above reasons, a satisfactory image stabiliser design is needed to miniaturise cell phone camera modules. In this work, the thermal actuating XY stage with four-axis system is designed and fabricated to achieve a low driving voltage and smaller IS shifting image stabiliser.

2. Structure design and fabrication: The novel feature of the proposed MEMS-based image stabiliser is a two-dimensional decoupling actuator, which is able to carry an IS. This device compensates for blurring when the human hand shakes. The designs of the XY stage are as follows.

2.1. Structure design: Since the mechanical coupling of the stage will induce nonlinear influences, the structure must be designed to achieve excellent decoupling effects; otherwise, to isolate actuating current and heat, the material SU-8 is patterned between the thermal actuator, position sensor and IS holder. Fig. 1 schematically depicts the design of the entire device; there are three signal output beams, one actuator, one position sensor and two decoupling beams in each direction. Since residual heat may change the operating frequency and cause nonlinear situations, the four-axis system is designed in this work; each hand-shake vector will be separated into two or three vectors in this system and compensated by the actuators. This compensating strategy will reduce the driving voltage, working temperature and residual heat in the XY stage.

2.2. Design of spring: Fig. 2 shows the three main types of flexure beams. Fig. 2*a* is a chevron thermal actuator. Since the pre-bending angle is small, it can be simplified as three clamped–clamped beams parallel to each other [12]. Equation (1) shows the stiffness

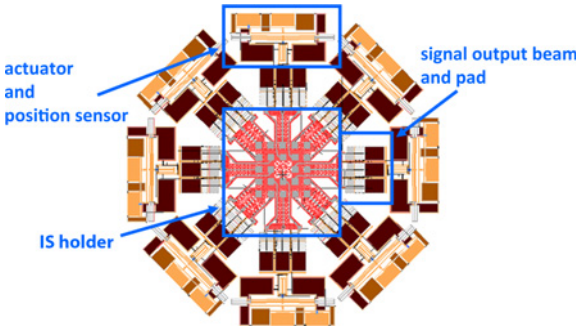

Figure 1 *Four-axis thermal actuating image stabiliser*

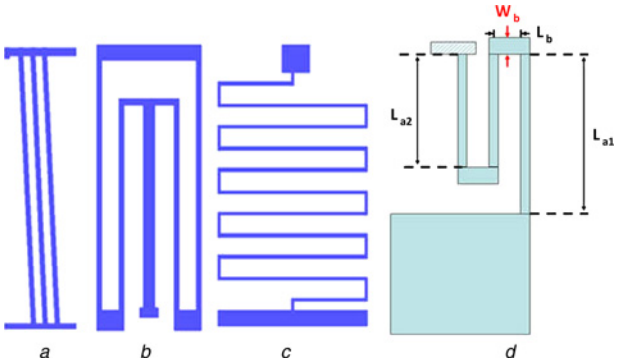

Figure 2 *Flexure beams*
a Thermal actuators
b Decoupling beams
c Signal output beams
d Illustration of folded-flexure spring

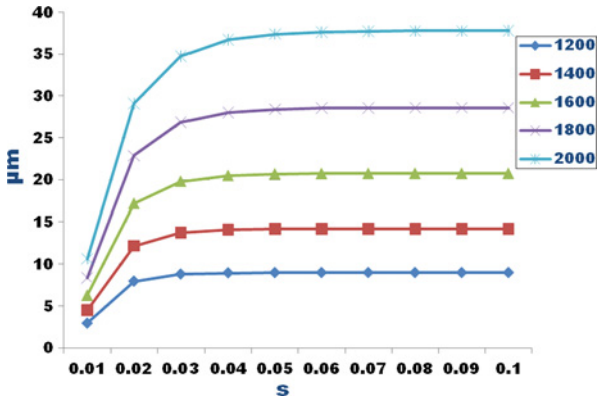

Figure 3 *Driving displacement of transient state on 20 V*

of a chevron thermal actuator:

$$kx_a = \frac{2Et_a w_a}{L_a}$$
$$ky_a = \frac{2Et_a w_a^3}{L_a^3} \quad (1)$$

where kx_a and ky_a are the stiffness of the actuator in the lateral direction and axis direction; E is Young's modulus of the decoupling flexure beam; and L_a, w_a and t_a are the length, width and thickness of the decoupling flexure beam, respectively. The stiffness ratio K_D of the decoupling beams can be expressed as (2):

$$K_D = \left|\frac{ky_a}{kx_a}\right| = \left(\frac{L_a}{w_a}\right)^2 \quad (2)$$

Fig. 2*b* is a decoupling beam, because lateral movement may induce instability and reduce linearity and reliability of thermal actuators. To avoid this situation, perfect isolation between different actuating directions is important. Because the folded beam has a large stiffness ratio, we can utilise it to reduce the mechanical interference from other directions. To prevent lateral displacement larger than the width of one pixel (about 2.5 μm) when the stage is driven to 25 μm, the decoupling ratio must be larger than 10.

Fig. 2*d* shows the spring design of the structure [13] when the driven force is parallel to the x-direction. The stiffness of a single folded-flexure spring under elastic deformation in the x-direction and the coupled stiffness in the y-direction are calculated as (3) and (4):

$$K_{xx} = \frac{48EI_aI_b(3I_bL_{a1} + I_aL_b)}{K_d} \quad (3)$$

$$K_{xy} = \frac{18EI_aI_b[2I_bL_{a1}(L_{a1} - L_{a2}) - I_aL_bL_{a2}]}{L_bK_d} \quad (4)$$

$$K_d = 3I_a^2L_b^2L_{a2}^2 + 6I_b^2L_{a1}(2L_{a1}^3 + L_{a2}^3) + 2I_aI_bL_b(8L_{a1}^3 + 6L_{a1}^2L_{a2} + 6L_{a1}L_{a2}^2 + L_{a2}^3) \quad (5)$$

where E is Young's modulus, I_a and I_b are the moments of inertia of the different beams, and L_a and L_b are the lengths of the different beams. Therefore when a single direction force is driven parallel to the x-direction, the decoupling ratio of x displacement to y displacement is defined as:

$$\left|\frac{K_{xy}}{K_{xx}}\right| = \frac{3[2I_bL_{a1}(L_{a1} - L_{a2}) - I_aL_bL_{a2}]}{4L_b(3I_bL_{a1} + I_aL_b)} \quad (6)$$

Fig. 3*c* shows a signal output beam. To output the signals of the IS, 24 beams are designed in this work, and the stiffness can be obtained by (3)–(5) as well.

Table 1 shows the length, width and height of the three-type flexure beams in Fig. 2.

2.3. Simulation: To design the chevron thermal actuator, the transient states of different lengths are simulated by CoventorWare, and the length, width, pre-bending angle and thickness of the actuator are 2000 μm, 20 μm, 3° and 50 μm. The simulation results are shown in Fig. 3, and we find that the actuators are proximately stable at 0.05 s.

3. Fabrication: The structure is fabricated by SOI process, as shown in Fig. 4. The thickness of the handle layer, isolation layer and device layer are 350, 2 and 50 μm individually, and the resistance of the device layer is about 0.02 Ω cm.

Utilising the ICP process, the structure, IS holder, signal output beams, thermal actuators and position sensors are fabricated on the SOI device layer. The signals isolation layer (nitride) and circuit routing (Al) are defined on the IS holder. Besides, the material SU-8 is defined between the actuating part and the IS holder to isolate driving current and heat. The scanning electron microscope (SEM) photographs of the sample device are shown in Figs. 5*a* and *b*. After SU-8 patterning, the suspending area of

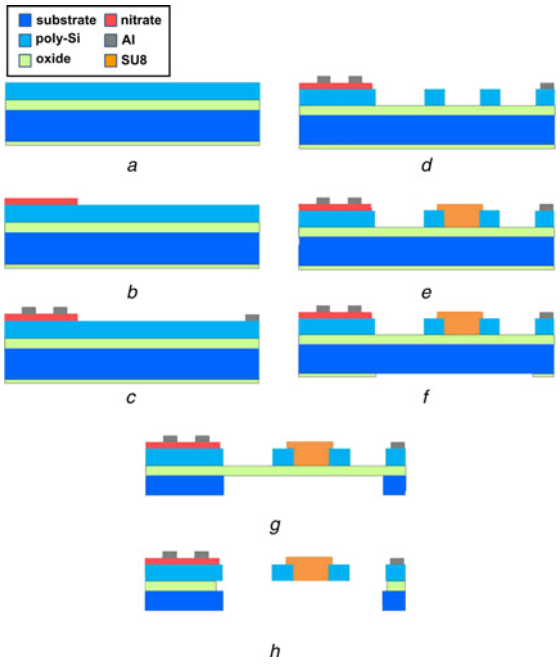

Figure 4 *Fabrication process of the XY stage*
a Backside oxide deposition (2 μm)
b Nitride patterning (0.5 μm)
c Al patterning (1 μm)
d Device layer patterning
e SU-8 patterning
f Backside oxide patterning
g Backside layer etching
h Release

Table 1 Specifications of flexure beams

Spring type	Fig. 3*a*, μm	Fig. 3*b*, μm	Fig. 3*c*, μm
Length	1000	*La*1:1000 *La*2:870	*La*1:670 *La*2:350
Width	20	20	15
Height	50	50	50

doi: 10.1049/mnl.2011.0100

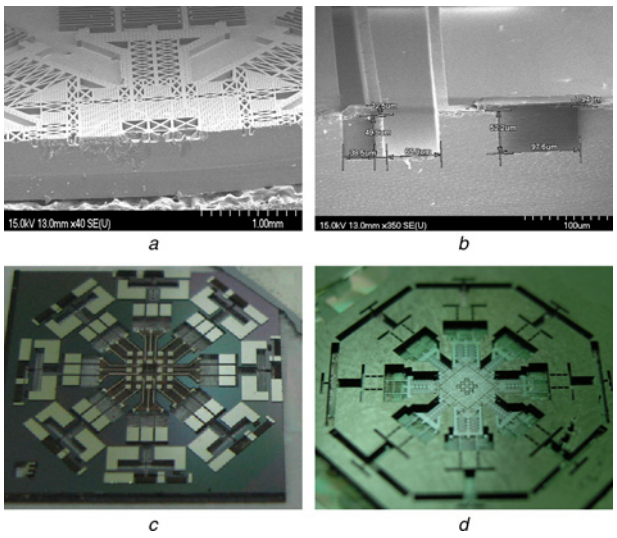

Figure 5 *Four-axis image stabiliser*
a IS holder
b SU-8 between IS holder and thermal actuator
c Stage top view
d Stage bottom view

the SOI backside is defined by the second ICP process, as shown in Figs. 5*c* and *d*.

The high-frequency (HF) vapour etching technique is finally employed to release the device structure. Device structures are released when the oxide layer is etched by the HF vapour. To protect the metal layer from HF vapour, the stage upper side is adhered to a silicon wafer by thermal release tape. After releasing, the wafer is heated to separate the device from the tape, then the IS bonding process starts. Figs. 6*a*–*d* depict the flip-chip bonder process; Figs. 6*a* and *b* show the alignment between bumps of the IS and the pads of the *XY* stage. After alignment, we supply 12 N pressure on the IS and reflow the stage to 230°C, as shown in Figs. 6*c* and *d*.

4. Measurement: Effectiveness of the image stabiliser was examined to evaluate the performance of the fabricated device. Fig. 7 shows the measurement results of the thermal image. The red and blue triangles represent the maximum and the minimum temperature of the thermal actuator when 10 V was supplied in 1 Hz. We can observe that the maximum temperature occurs in the middle of the actuator and the pads are close to room temperature.

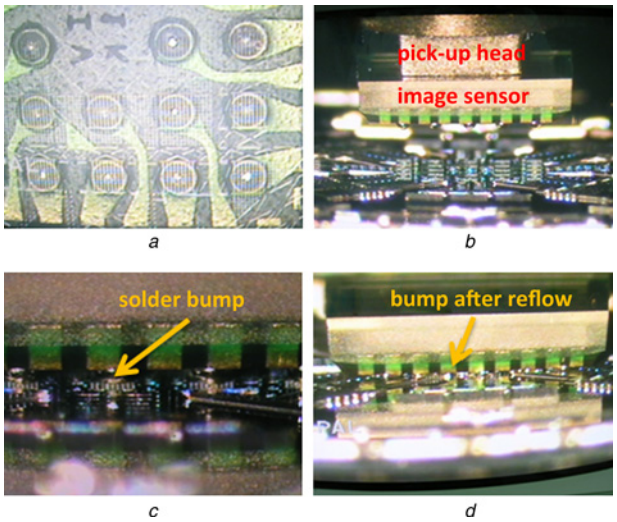

Figure 6 *Flip-chip bonding process of the image stabiliser*

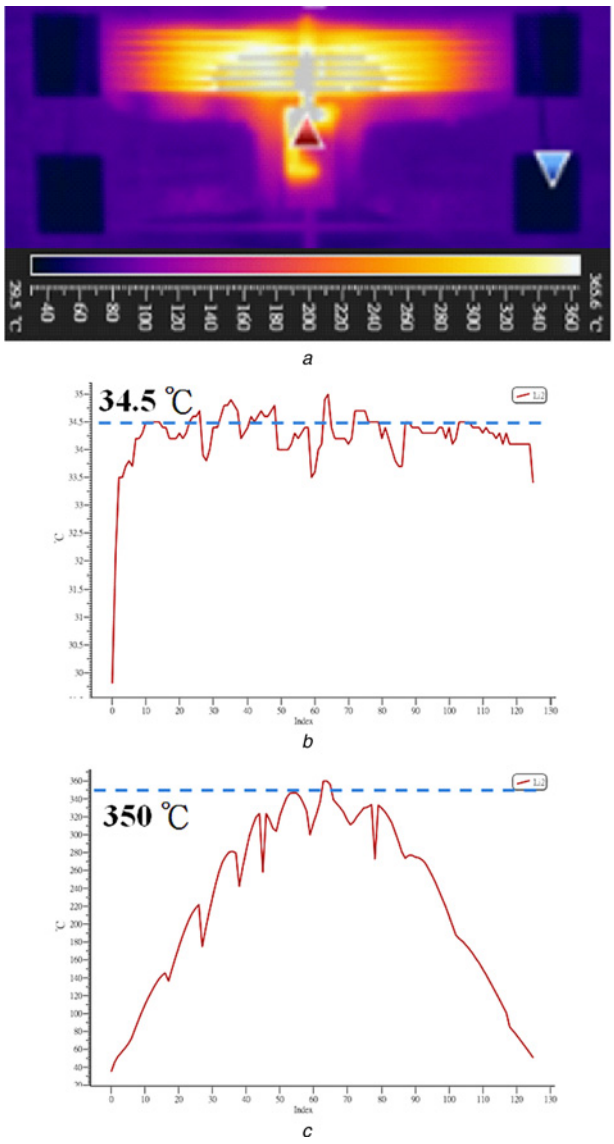

Figure 7 *Measurement result of thermal image in 10 V 1 Hz*
a Thermal actuator
b Temperature profile in on-state
c Temperature profile in off-state

Figs. 7*b* and *c* show the temperature profile between both side pads in on-state and off-state, the maximum temperature is approximate to 350°C in on-state and 34.5°C in off-state.

During the static driving test, the actuator was driven by a DC voltage, and displacement of the actuator was measured by a MEMS motion analyser (MMA). When a 20 V driving voltage was supplied on the proposed device in the *y*-direction, moving displacement in the *y*-direction is 33 μm with 1.78 μm displacement along the *x*-direction, as shown in Fig. 8*a*, and the experimental decoupling

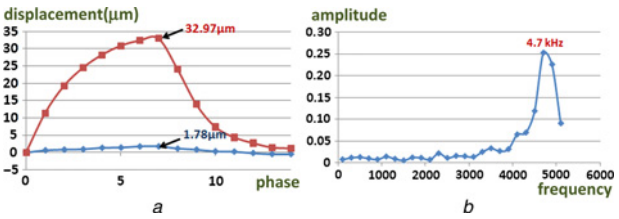

Figure 8 *MMA measurement results*
a Displacement of *x*- and *y*-direction on 20 V
b Resonant frequency

ratio can be calculated to 18.54, which conforms to the system requirement. In the dynamic characterisation, we also use the MMA system to evaluate the resonant frequency, as shown in Fig. 8*b*, and we can observe that the resonant frequency approximates to 4.7 kHz.

5. Conclusion: In this work we designed, simulated and fabricated a novel four-axis thermal actuating image stabiliser and found the way to miniaturise the stage size but without needing to enlarge the size of the power circuits. Besides, utilising the MEMS process and the four-axis actuating strategy to fabricate and control the image stabiliser not only miniaturises the device size, but also decreases the driving voltage and the size of the power chip.

6. Acknowledgments: This work was supported in part by the Ministry of Economic Affairs, Taiwan, under contract 97-EC-17-A-07-S1-011, and the National Science Council, Taiwan, under contract NSC-98-2220-E-009-014, NSC-98-2220-E-009-032 and NSC-98-2218-E-039-001. It was also supported in part by the Taiwan Department of Health Clinical Trial and Research Center of Excellence under contract DOH99-TD-B-111-004 and DOH99-TD-C-111-005 and the National Science and Technology Program for SOC under contract NSC-97-2220-E-009-044. Simulation software support was received from the National Center for High-Performance Computing, Taiwan.

7 References

[1] Sun L., Wang J., Rong W., Li X., Bao H.: 'A silicon integrated micro nano-positioning *XY*-stage for nano-manipulation', *J. Micromech. Microeng.*, 2008, **18**, p. 125004

[2] Takahashi K., Mita M., Fujita H., Toshiyoshi H.: 'A high fill-factor comb-driven *XY*-stage with topological layer switch architecture', *IEICE Electron. Express*, 2006, **3**, pp. 197–202

[3] Kwon H.N., Lee J.-H., Takahashi K., Toshiyoshi H.: 'Micro *XY* stages with spider-leg actuators for two-dimensional optical scanning', *Sens. Actuators A*, 2006, **130–131**, pp. 468–477

[4] Kwon S., Lee L.P.: 'Stacked two dimensional micro-lens scanner for micro confocal imaging array'. Proc. IEEE MEMS '02, 2002, pp. 483–486

[5] Laszczyk K., Bargiel S., Gorecki C., Krezel J.: 'Towards integration of glass microlens with silicon comb-drive *X-Y* microstage'. IEEE/LEOS Int. Conf. Optical MEMS and Nanophotonics, 2008, pp. 168–169

[6] Yasumura K.Y., Grade J.D., Jerman H.: 'Fluid damping of an electrostatic actuator for optical switching applications'. Proc. Solid-State Sensor, Actuator and Microsystems Workshop, 2002, pp. 358–361

[7] Takahashi K., Kwon H.N., Mita M., *et al.:* 'A silicon micromachined f-θ microlens scanner array by double-deck device design technique', *IEEE J. Sel. Top. Quantum. Electron.*, 2007, **13**, pp. 277–282

[8] Chiou J.C., Hung C.-C., Lin C.-Y.: 'Design, fabrication, and actuation of MEMS-based image stabilizer for photographic cell phone applications', *J. Micromech. Microeng.*, 2010, **20**, (7), article id. 075025

[9] Chiou J.C., Hung C.-C., Lin C.-Y., Lin Y.J.: 'Design, fabrication, and actuation of MEMS-based image stabilizer', *Jpn. J Appl. Phys.,* 2010, **49**, article id. 014201

[10] Yang J.P., Mou J.Q., Chong N.B., *et al.:* 'Probe recording technology using novel MEMS devices', *Microsyst. Technol.*, 2007, **13**, pp. 733–740

[11] Lee C.-C., Chen W.-C., Lee S.-Y., Fang W.: 'Design and implementation of a novel polymer joint for thermal actuator current and thermal isolation'. IEEE MEMS Conf., 2010, pp. 156–159

[12] Legtenberg R., Groeneveld A.W., Elwenspoek M.: 'Comb-drive actuators for large displacements', *J. Micromech. Microeng.*, 1996, **6**, pp. 320–329

[13] Wu J., Yue R., Zeng X., Kang M., Wang Z., Liu L.: 'An open-configuration electrowetting-based biofluidics actuation for preventing biomolecular adsorption'. Proc. 1st IEEE Int. Conf. Nano/Micro Engineered and Molecular Systems, NEMS '06, Zhuhai, China, 18–21 January 2006, pp. 1152–1155

doi: 10.1049/mnl.2011.0100